Boosting Monocular Depth Estimation with Sparse Guided Points*

Guangkai Xu[1], Wei Yin[2], Hao Chen[3], Kai Cheng[1], Feng Zhao[1], Chunhua Shen[3]

[1] University of Science and Technology of China [2] The University of Adelaide [3] Zhejiang University

Abstract

Existing monocular depth estimation shows excellent robustness in the wild, but the affine-invariant prediction requires aligning with the ground truth globally while being converted into the metric depth. In this work, we firstly propose a modified locally weighted linear regression strategy to leverage sparse ground truth and generate a flexible depth transformation to correct the coarse misalignment brought by global recovery strategy. Applying this strategy, we achieve significant improvement (more than 50% at most) over most recent state-of-the-art methods on five zero-shot datasets.

Moreover, we train a robust depth estimation model with 6.3 million data and analyze the training process by decoupling the inaccuracy into coarse misalignment inaccuracy and detail missing inaccuracy. As a result, our model based on ResNet50 even outperforms the state-of-the-art DPT ViT-Large model with the help of our recovery strategy. In addition to accuracy, the consistency is also boosted for simple per-frame video depth estimation. Compared with monocular depth estimation, robust video depth estimation, and depth completion methods, our pipeline obtains state-of-the-art performance on video depth estimation without any post-processing. Experiments of 3D scene reconstruction from consistent video depth are conducted for intuitive comparison as well. Code is available at github: AdelaiDepth

1. Introduction

Dense monocular depth estimation [29, 30, 54] is a significant task and can be helpful in many fields such as autonomous driving [42], virtual reality (VR) [18], augmented reality (AR), and 3D scene reconstruction [49]. Despite the excellent robustness of monocular depth estimation in the wild, existing state-of-the-art methods can only predict affine-invariant depth with unknown scale and shift, which requires aligning with the ground truth through global least-square fitting.

However, the precious ground truth is often obtained from expensive sensors like 3D laser scanning device. Cost-effective sensors can also provide ground truth but partially inaccurate, which may bring in extra decrease for the performance. What is more, the accuracy of aligned prediction depth cannot be further improved with the increase of ground truth points.

To leverage the precious ground truth and enhance the performance, we first analyze the error map between the ground truth and aligned prediction depth, and observe that the error can be decoupled into two parts: the coarse misalignment error and detail missing error. The latter can only be alleviated by supervision during training or optimization during post-processing, but the former can be reduced by fitting the distribution of prediction depth and ground truth more flexibly.

In this work, we propose to quantitatively decouple the above-mentioned inaccuracy and alleviate the coarse misalignment error by fitting a depth transformation with sparse ground-truth depth through a modified locally weighted linear regression strategy. Compared with traditional linear regression, the proposed strategy can leverage the robust depth prior of monocular depth estimation and the distribution of ground truth to improve the performance. Ablation study shows our strategy is robust to both the amount and randomly-generated noises of the ground truth, which can also perform well with ground-truth obtained from cost-effective sensors and even some traditional geometric algorithm such as triangulation.

Besides leveraging sparse ground truth, the robustness of monocular depth estimation can also bring a precise prior, boost the performance, and reduce the demand for sparse points. Therefore, *a robust model trained with 6.3 Million data is proposed and analyzed* in our experiments. With the robust data-driven model, modified recovery strategy, and sparse guided points, a novel pipeline for video depth estimation is proposed by simply predicting per-frame depth and aligning with a sparse set of ground-truth depth values.

To summarize, our main contributions are as follows:

- A novel metric depth recovery strategy that can significantly improve the performance of consistency and accuracy but only requires sparse guided depth.

*The first three authors contributed equally. Part of this work was done when GX, HC, KC were with Huawei; and CS was with The University of Adelaide.

- An effective tool based on scale recovery to visualize and quantify monocular depth errors caused by coarse misalignment and missing details, respectively.
- A robust monocular depth estimation model trained on diverse dataset collectives of 6.3 Million images in total, together with detailed analysis of its performance *w.r.t.* the training dataset size using our analytics tool.
- A pipeline for consistent and accurate video depth estimation, assisted with very sparse depth information.
- With our local scale and shift recovery method, we systematically analyze the error distribution for depth estimation in many settings, including single image depth estimation, depth completion and video depth estimation methods and show consistent precision gain.
- Experiments are conducted to apply modified local recovery strategy to state-of-the-art monocular depth estimation methods, bringing more than 50% improvement in performance over all state-of-the-art methods.

With the proposed strategy, our ResNet50 model even outperforms DPT [29] with the ViT-Large [10] backbone. For video depth estimation, our pipeline significantly improves both the accuracy and consistency, and achieves state-of-the-art on five NYU [34] videos. 3D scene reconstructions from consistent video depth estimation are also conducted for intuitive comparison.

2. Related Work

Monocular Depth Estimation. Monocular depth estimation is an important problem. Through training a dataset individually, many methods [20, 21, 52] have achieved promising results. However, the resulting models generalize poorly to diverse scenes. To mitigate this problem, Chen *et al*. [2] constructed the first large-scale and diverse dataset (DIW), and enforced the network to learn depth ordering relations, termed relative depth. As very sparse paired points are annotated in each image, several approaches [2, 4, 22, 43, 44] propose to obtain the ground truth of dense relative depth by leveraging the online web-stereo videos or images. Owing to large-scale and diverse data samples, these strategies can produce a model with strong generalization.

Although learning relative depth can obtain a robust model, the relative depth can only represent ordinal depth relations and loses the geometry information, *i.e.*, one point is farther or closer than another one. Therefore, some works [30, 51, 53, 54] proposed to learn affine-invariant depth. Ranftl *et al*. [30] proposed the scale-shift invariant loss to leverage the training on multi-source data, which can achieve promising generalization on diverse scenes. Yin *et al*. [54] employ a heterogeneous loss training strategy, which obtains state-of-the-art performance on multiple zero-shot testing datasets. Our method is built upon these robust depth estimation methods on different RGB-D datasets for the generalization and detail recovery ability. We also go one step further to remedy the issue of scale-missing by devising a powerful local scale recovery technique with additional easy-access information.

RGB-D Datasets. Datasets [9, 32, 35, 38] are significant for the advancement of data-driven depth prediction methods. Current datasets can be summarized into two categories according to their quality. Some datasets are captured by RGB-D sensors, which can retrieve accurate metric depth. Make3D [32] is the first outdoor RGB-D dataset constructed for monocular depth prediction study. KITTI and NYU are captured by LIDAR on outdoor streets and Kinect in indoor rooms. Larger-scale RGB-D datasets are also constructed, such as ScanNet [9], Taskonomy [55], DIML [7], and DIODE [38]. These datasets usually contain very limited scenes only.

To compress more diversified scenes, some algorithms try to leverage online images and videos. Chen *et al*. [2] constructed the largest RGB-D dataset, where the ground-truth depth maps were manually annotated with only one pair of ordinal relations. MegaDepth [22] employs structure from motion to construct the depth supervision on the still and rigid scenes. To include more non-rigid and diverse scenes, Xian *et al*. [43] and Wang *et al*. [39] adopted optical flow techniques to build datasets of relative depth. Chen *et al*. [4] released the diverse OASIS dataset, which contains both ordinal depth annotations and camera intrinsic parameters. Yin *et al*. [51, 53] propose another large-scale and diverse RGB-D datasets: DiverseDepth.

Depth Completion. Depth completion aims to recover a dense depth map from a very sparse input. Some methods [3, 5, 6, 28, 50] combine the RGB texture information with sparse depth together to solve the problem. Promising results have been obtained on KITTI and NYU benchmarks. Except for these very sparse depth types, commodity-level RGB-D cameras such as Kinect, RealSense, and Tango produce depth images that are semi-dense but missing certain regions. Several methods treat this as a depth inpainting task and leverage smoothness priors [16], background surface extrapolation [27], and surface normals [57]. Our method can be considered as an alternative approach to depth completion but requires much less guided points.

Video-based Depth Estimation. Video-based depth estimation has attracted extensive attentions recently. They are mainly categorized into multi-view stereo based approaches [11, 24, 36] and hybrid methods [19, 25]. The former try to improve the traditional structure-from-motion and multi-view stereo pipeline with some learning-based modules, such as a differentiable depth and pose modules or a depth estimation uncertainty predictor. Such methods are all based on a cost volume that is constructed by warping neighboring frames to a reference viewpoint. Although

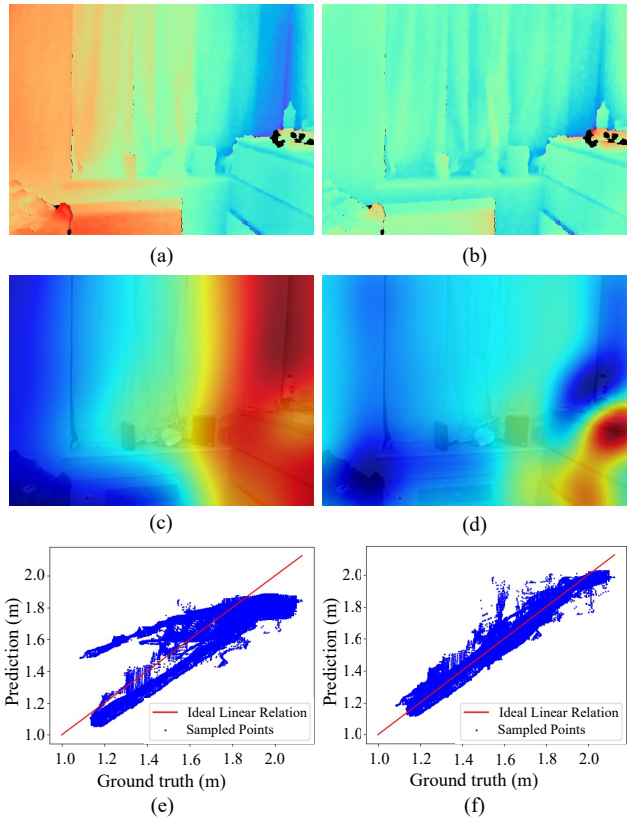

Figure 1. Per-pixel error map of ground truth depth and predicted depth aligned through (a) global recovery and (b) local recovery separately. (c) The scale map and (d) shift map of local recovery. Distribution of prediction-ground truth pairs obtained through (e) global recovery and (f) local recovery separately.

promising results have been achieved, they may fail to handle dynamic scenes. By contrast, the hybrid method aim to combine single-view depth estimation and multi-view stereo for achieving geometrically consistent video depth. In this work, through per-frame prediction and alignment with guided points, we can obtain consistent video depth prediction.

3. Our Method

3.1. Metric Depth Recovery Strategy

Current monocular depth estimation [29,30,51,54] methods have achieved promising results on diverse scenes. The problem is that their predicted depth is scale-shift-invariant, termed affine-invariant depth/inverse depth [51, 53]. To recover the metric depth, it should be scaled and shifted, *i.e.*, $d^* = ds + \mu$, where d, s, and μ are the predicted affine-invariant depth, scale, and shift respectively. Current methods propose to obtain the scale and shift through a global least-squares fitting method using some ground-truth depth:

$$\begin{aligned} &\min_{\boldsymbol{\beta}} \sum_{i=1}^{n} [y_i - \boldsymbol{\beta} \boldsymbol{x}_i^{\mathsf{T}}]^2, \\ &\boldsymbol{\beta} = [s, \mu] \in \mathcal{R}^{1\times 2},\ \boldsymbol{x}_i = [d_i, 1]\ \in \mathcal{R}^{1\times 2} \\ &\hat{\boldsymbol{\beta}} = (\boldsymbol{X}^{\mathsf{T}}\boldsymbol{X})^{-1}\boldsymbol{X}^{\mathsf{T}}\boldsymbol{y} \end{aligned} \tag{1}$$

where $\boldsymbol{y}$ is the ground-truth metric depth, $\boldsymbol{X}$ is the homogeneous representation of the predicted depth d. The optimized scale and shift are $\hat{\boldsymbol{\beta}}$.

The problem is that such a globally scaling and shifting method cannot diminish spatially heterogeneous errors, which always follows a rather simple pattern. For example, we visualize the pixel-wise absolute error map between ground truth and the predicted depth with the recovered scale and shift, see Fig. 1(a). We observe that such a globally recovering method cannot remove the spatial error. The left part shows higher error than that of the right part. Motivated by this observation, we propose to leverage a local recovering method. Guided by very sparse ground truth points, we can use simple regression models, *i.e.*, *locally weighted linear regression (LWLR)*, to fit these error maps. Thus, we propose an effective strategy to quantify and fix these low-rank spatial errors which are common in depth estimation.

Locally Weighted Linear Regression. We propose to employ a modified locally weighted regression method, which can assess the spatial heterogeneity in the estimated relationships between the independent and dependent variables. The original method is illustrated as follows.

$$\begin{aligned} &\min_{\boldsymbol{\beta}_{u,v}} \sum_{i=1}^{m} [y_i - \boldsymbol{\beta}_{u,v} \boldsymbol{x}_i^{\mathsf{T}}]^2 \cdot w_{i,u,v}, \\ &\boldsymbol{\beta}_{u,v} = [s_{u,v}, \mu_{u,v}] \in \mathcal{R}^{1\times 2},\ \boldsymbol{x}_i = [d_i, 1] \in \mathcal{R}^{1\times 2} \\ &\hat{\boldsymbol{\beta}}_{u,v} = (\boldsymbol{X}^{\mathsf{T}}\boldsymbol{W}_{u,v}\boldsymbol{X})^{-1}\boldsymbol{X}^{\mathsf{T}}\boldsymbol{W}_{u,v}\boldsymbol{y} \end{aligned} \tag{2}$$

Here, $\boldsymbol{y}$ represents the ground-truth metric depth of sparse guided points (we use around 25$\sim$100 points in practice), $\boldsymbol{X}$ is the homogeneous representation of the predicted depth d at these guided points, $\boldsymbol{\beta}_{u,v}$ is the scale and shift at the image location (u, v). $\boldsymbol{W}_{u,v}$ is a weight matrix. Such a weight matrix gives the most weight to the data points closest to the point of estimation and the least weight to the data points that are the furthest away. The use of the weights is based on the idea that points near each other in the explanatory variable space are more likely to be related to each other in a simple way than points that are further apart. In our implementation, we employ a Gaussian kernel function.

$$w_{i,u,v} = \frac{1}{\sqrt{2\pi}} \exp\left(-\frac{d_{i,u,v}^2}{2b^2}\right) \tag{3}$$

where b is the bandwidth of the Gaussian kernel, and $d_{i,u,v}$

is the Euclidean distance between the guided point (u_i, v_i) and target point (u, v).

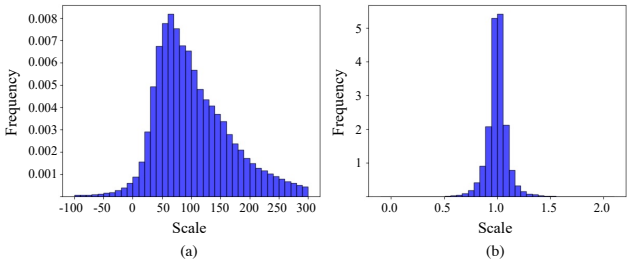

Figure 2. Distribution of recovered scales with locally weighted linear regression methods. (a) Scale distribution of original algorithm in Eq. (2), which contains negative values and spreads widely. (b) Scale map of our proposed algorithm in Eq. (4), which is positive and reasonable.

Such obtained scale map and shift map can yield much more accurate metric depth than the previous global methods. However, we observe that some values of the scale map can be fitted to negative due to the shift-invariant characteristic of monocular depth and flexibility of the weighted linear regression, which inverses the distribution of depth prediction and lacks reasonableness. The distribution of scale is shown in Fig. 2(a). Since the bias is not centered and the solution space is not bounded, results are wildly distributed with no physical meanings and far from the real scale and shift. Therefore, we proposed to align monocular depth with sparse ground truth first, and restrict the solution to be simple by adding an ℓ_2 regularization on the shift.

$$\begin{aligned} &\min_{\boldsymbol{\beta}_{u,v}} \sum_{i=1}^{m} [y_i - \boldsymbol{\beta}_{u,v} \boldsymbol{x}_i^{\mathsf{T}}]^2 w_{i,u,v} + \lambda [\boldsymbol{\beta}_{u,v}[1]]^2, \\ &\boldsymbol{\beta}_{u,v} = [s_{u,v}, \mu_{u,v}] \in \mathcal{R}^{1\times 2}, \boldsymbol{x}_i \ \in \mathcal{R}^{1\times 2} \\ &\hat{\boldsymbol{\beta}}_{\boldsymbol{u,v}} = (\boldsymbol{X}^{\mathsf{T}} \boldsymbol{W}_{u,v} \boldsymbol{X} + \boldsymbol{A})^{-1} \boldsymbol{X}^{\mathsf{T}} \boldsymbol{W}_{u,v} \boldsymbol{y}, \\ &\boldsymbol{A} = \begin{bmatrix} \lambda & 0 \\ 0 & 0 \end{bmatrix} \end{aligned} \tag{4}$$

where, $\boldsymbol{\beta}_{u,v}[1]$ is the shift value at point (u, v). With the regularizer of shift, the location-related scale map is encouraged to be positive and reasonable, as shown in Fig. 2(b). Finally, with the optimized scale and shift at location (u, v), we can obtain its metric depth $d^*_{u,v} = s_{u,v} \cdot d + \mu_{u,v}$.

With our proposed local recovery strategy, we only need a very sparse set of ground-truth depth values (around 25$\sim$100 points) to recover the metric depth map by fitting a location-related scale map and a shift map. Fig. 1 compares the global least-square fitting and our proposed weighted linear regression results. Owing to optimized pixel-wise scale map (Fig. 1(c)) and shift map (Fig. 1(d)), the overall loss is reduced *significantly* (Fig. 1(b)). Note that the predicted affine-invariant depths are the same for two methods. Importantly, the recovered metric depth with our method is highly linear correlated to the ground truth (see Fig. 1(e) and Fig. 1(f)).

Dataset	# images	Scene	Quality
Taskonomy [56]	4.5M	Indoor	High-quality
ApolloScape [40]	114K	Outdoor	High-quality
Hypersim [31]	298K	Indoor	High-quality
GraspNet [12]	82K	Indoor	High-quality
Tartanair [41]	289K	Synthetic	High-quality
UASOL [1]	162K	Outdoor	Mid-quality
DrivingStereo [48]	182K	Outdoor	Mid-quality
DIML [8]	121K	Outdoor	Mid-quality
HoloPix50k [17]	99K	Indoor	Low-quality
KeystoneDepth [26]	74K	In the wild	Low-quality
WSVD [39]	117K	In the wild	Low-quality
HRWSI [45]	18K	Outdoor	Low-quality
MegaDepth [22]	79K	Outdoor	Low-quality
DiverseDepth [53]	90K	In the wild	Low-quality
Total	6.3M	-	-

Table 1. Diverse training data used in our experiment.

3.2. Boosting Monocular Depth and Monocular Video Depth Estimation

In this work, following LeReS [54], we collect over **6.3 Million** data to train a strong and robust monocular depth estimation model. With only around one hundred points, we can obtain very accurate metric depth. Comparing to existing depth completion methods [5, 28], which take sparse points as input for learning, our method is a simple and effective learning-free post process. It can be easily plugged to any monocular depth estimation and completion methods to boost performance.

Furthermore, our recovery strategy and strong model can be combined to solve the video depth estimation problem. Current video depth estimation methods mainly try to leverage inter-frame consistency or multi-view geometry constraints. We observe that performing per-frame prediction and the scale-shift alignment with very sparse guided points, we can obtain accurate and consistent metric video depth prediction.

Consistency Metric for Video Depth Estimation. We propose the average distortion distance (ADD) error to evaluate the consistency of predicted video depths. The predicted depths of consecutive frames are unprojectd to 3D space and establish their correspondence with known camera poses, intrinsic parameters and ground-truth depth. The average distortion distance (ADD) measures the average

Method	Backbone	KITTI		NYU		ScanNet		ETH3D		DIODE	
		AbsRel↓	δ_1↑	AbsRel↓	δ_1↑	AbsRel↓	δ_1↑	AbsRel↓	δ_1↑	AbsRel↓	δ_1↑
OASIS [4]	ResNet50	31.7	43.7	21.9	66.8	19.8	67.9	29.2	59.5	48.4	53.4
MegaDepth [23]	ResNet50	20.1	63.3	19.4	71.4	19.0	71.2	26.0	64.3	39.1	61.5
Xian *et al*. [44]	ResNet50	27.0	52.9	16.6	77.2	18.9	71.4	26.1	61.9	35.8	63.8
WSVD [39]	ResNet50	24.4	60.2	22.6	65.0	18.9	71.4	26.1	61.9	35.8	63.8
Chen *et al*. [3]	ResNet50	32.7	51.2	16.6	77.3	16.5	76.7	23.7	67.2	37.9	66.0
DiverseDepth [51]	ResNet50	19.0	70.4	11.7	87.5	10.8	88.2	22.8	69.4	37.6	63.1
LeReS [54]	ResNext101	14.8	78.6	8.6	92.1	9.5	91.2	9.7	90.3	21.6	80.8
MiDaS-large [30]	ResNext101	13.4	81.9	10.2	90.0	9.8	90.9	10.1	90.5	19.0	76.1
DPT-large [29]	ViT-Large	10.0	90.1	9.8	90.3	7.8	93.8	7.8	94.6	18.2	75.8
Ours(global)	ResNet50	10.9	88.5	8.2	92.6	8.9	92.0	8.4	92.1	22.0	80.1
Ours(local)	ResNet50	**5.7** (−48%)	**95.4**	**4.7** (−43%)	**96.9**	**4.3** (−52%)	**97.4**	**5.0** (−40%)	**96.6**	**16.5** (−25%)	**85.2**

Table 2. Quantitative comparison of monocular depth estimation with state-of-the-art methods on five unseen datasets. 'global' and 'local' represents global and our proposed local metric depth recovery strategy separately. For global strategy, our ResNet50 [15] model outperforms other ResNet50 and ResNeXt101 [47] models on four test datasets. With our proposed local recovery and 100 sparse ground truth, our ResNet50 model achieves significant improvement and outperforms state-of-the-art DPT [29] with the ViT-large [10] backbone.

Method	KITTI		NYU		ScanNet		ETH3D		DIODE	
	AbsRel↓									
	before	after	before	after	before	after	before	after	before	after
LeReS [54]	14.8	8.0 (−46%)	8.6	4.8 (−44%)	9.5	4.4 (−54%)	9.7	5.6 (−42%)	21.6	16.2 (−25%)
MiDaS-large [30]	13.4	6.2 (−54%)	10.2	5.1 (−50%)	9.8	4.3 (−56%)	10.1	4.9 (−52%)	19.0	14.5 (−24%)
DPT-large [29]	10.0	5.2 (−48%)	9.8	5.0 (−49%)	7.8	3.8 (−51%)	7.8	4.2 (−54%)	18.2	14.3 (−21%)
NLSPN [28]	-	-	3.7	3.3 (−11%)	-	-	-	-	-	-
VNL [52]	-	-	10.6	4.0 (−62%)	-	-	-	-	-	-
Monodepth2 [14]	8.1	6.1 (−25%)	-	-	-	-	-	-	-	-

Table 3. Boosting various monocular depth estimation with our local recovery method. We compare the accuracy without (see 'before' columns) and with (see 'after' columns) our recovery methods. We can see the performance of all these monocular depth estimation (such as VNL [52], Monodepth2 [14], DPT [29], and so on) and depth completion (NLSPN [28]) methods are boosted significantly.

distance of paired 3D points:

$$\text{ADD} = \frac{1}{n}\sum_{j=1}^{n}\|\boldsymbol{c}_{1j} - \boldsymbol{c}_{2j})\|_2^2 \qquad (5)$$
$$\boldsymbol{c}_{ij} = \boldsymbol{R}_i\boldsymbol{K}_i^{-1}d(\boldsymbol{p}_{ij})\widetilde{\boldsymbol{p}}_{ij} + \boldsymbol{T}_i,\ i = 1, 2$$

Here, $\boldsymbol{c}_{ij}$ is the 3D coordinates of paired point j in frame i, $\boldsymbol{p}_{ij}$ is the 2D pixel location, $\widetilde{\boldsymbol{p}}_{ij}$ is its homogeneous representation. $d(\boldsymbol{p}_{ij})$ is the prediction depth of $\boldsymbol{p}_{ij}$, and $\boldsymbol{K}_i$, $\boldsymbol{R}_i$, $\boldsymbol{T}_i$ represents the intrinsic parameters, rotation, and translation of frame i, respectively.

4. Experiments

Training Datasets. To train a robust monocular depth estimation model, 6.3 million diverse RGB-D pairs are processed and trained following the previous work LeReS [54], and the composition of datasets is listed in Table 1.

Implementation Details. Following [51, 54], we balance high-quality, middle-quality, and low-quality data in each batch to ensure that they accounts for almost the same ratio in each batch. For example, each data accounts for $N/3$ if the batch size is set to N during training. Multiple data augmentation techniques are used, such as random flipping, color transformations, image blur and so on. We randomly crop the image by 448×448 for training. ResNet50 [15] with ImageNet pretrained weight is adopted in our experiments. We use SGD with momentum, starting with a learning rate of 0.04. It is decayed with 0.1 for 4 times. The batch size is set to 128.

Evaluation Details. We evaluate the absolute mean relative error (AbsRel error) and the percentage of pixels with

$$\delta_1 = \max\left(\frac{d_{pred}}{d_{gt}}, \frac{d_{gt}}{d_{pred}}\right) < 1.25$$

on 5 zero-shot datasets including KITTI [13], NYU [34], ScanNet [9], ETH3D [33] and DIODE [38].The consistency evaluation experiments of video depth estimation and 3D scene reconstruction are performed on 5 NYU videos. Besides the AbsRel error metric and δ_1, the average distortion distance (ADD) proposed in Sec. 3.2 is also evaluated to show the video depth consistency.

4.1. Monocular Depth Estimation

Comparison with State-of-the-art Methods. In this experiment, we compare with state-of-the-art robust monoc-

Training Data	KITTI	NYU	ScanNet AbsRel↓	ETH3D	DIODE
Global Recovery					
42K	14.1	11.0	11.8	9.5	23.2
352K	15.0	9.2	10.0	9.4	22.1
900K	11.5	8.6	9.7	9.0	21.6
3.8M	11.1	8.2	8.9	8.4	21.9
6.3M	10.9	8.2	8.9	8.4	22.0
Local Recovery					
42K	6.9 (−51%)	5.8 (−47%)	5.2 (−56%)	5.9 (−38%)	16.9 (−27%)
352K	7.3 (−51%)	5.2 (−43%)	4.7 (−53%)	6.2 (−34%)	16.6 (−25%)
900K	5.8 (−50%)	4.9 (−43%)	4.6 (−53%)	5.4 (−40%)	16.3 (−25%)
3.8M	5.8 (−48%)	4.7 (−43%)	4.3 (−52%)	5.2 (−38%)	16.5 (−25%)
6.3M	5.7 (−48%)	4.7 (−43%)	4.3 (−52%)	5.0 (−40%)	16.5 (−25%)

Table 4. Ablation study for training data of our robust depth estimation module. With the increase of data, the performance of depth estimation improves gradually.

Amount	Distribution	Noise	b	NYU AbsRel↓	NYU δ_1↑
10×10	Grid	0%	50	4.8	96.4
5×5	Grid	0%	50	5.8	94.7
20×20	Grid	0%	50	4.6	96.7
10×10	Grid	0%	25	4.7	96.0
10×10	Grid	0%	100	5.8	95.5
10×10	Grid	10%	50	5.5	96.2
10×10	Grid	20%	50	6.8	95.5
100	Uniform (whole image)	0%	50	4.3	97.0
100	Uniform (half image)	0%	50	11.3	87.6

Table 5. Ablation study for parameters of our proposed local recovery strategy. Amount, distribution and error correspond to the number, the distribution and the perturbation percentage of sampled ground-truth. Parameter b represents the bandwidth of the Gaussian kernel function.

ular depth estimation methods on five zero-shot datasets. Their scale and shift are recovered with a globally least-square fitting method. Note that we use their released weight for evaluation, and the results are shown in Table 2. Our method with the ResNet50 backbone, recovering the scale and shift with the proposed locally weighted linear regression method ('Ours (local)'), can outperform all previous methods by a large margin over all zero-shot testing datasets. Note that our training data is comparable to that of DPT and DPT used a much stronger transformer backbone (ViT-large [10]). Furthermore, our locally scale-shift recovering method is better than previous global method ('Ours (global)') significantly.

Effectiveness of Locally Weighted Linear Regression and Decoupling of Monocular Depth Error. To demonstrate our proposed locally weighed linear regression can boost various monocular depth estimation methods, we enforce it on multiple different methods: 1) learning affine-invariant depth methods, *e.g.*, LeReS [54], MiDaS [30], and DPT [29]; 2) learning metric depth on a specific dataset (VNL [52]); 3) learning scale-invariant depth with unsupervised methods (MonoDepth2 [14]); 4) depth completion method (NLSPN [28]). Results are shown in Table 3. We uniformly sample 100 guided points to do the local recovery. All their performances are boosted significantly (see the 'after' columns). Critically, the NLSPN method has input such 100 sampled points for completion, but our method can still further boost its performance. Note that we used their released weights and code for this experiment.

Besides improving performance, local recovery strategy is also performed to decouple monocular depth error between ground truth and global aligned prediction into coarse misalignment error and detail missing error. Compared with the error of global recovery, the alleviated error in percentage brought by local recovery represents the coarse misalignment error.

Ablation Study for Training Data. In this experiment, we aim to study the relations between the data volume and performance improvement. We gradually aggregate more data for training, and evaluate the performance on 5 zero-shot datasets. Note that 3 different quality data sources are increased in balance, and the results are illustrated in Table 4. We can observe that when the data size increases from 42k to 900K (around by 20 times), the performance is boosted significantly. However, when further increasing by 7 times, the accuracy can only be improved slightly. We conjecture that such a large-scale data has fully exploited the capacity of the model (ResNet50 backbone).

Furthermore, we also conduct local recovery here to decouple the error into coarse misalignment error and detail missing error, as mentioned in the last paragraph. As shown in Table 4, the percentage of coarse misalignment error remains nearly constant, which shows the model can study the detail information and the global structure simultaneously. Fig. 3 shows an overall decrease of mean average error and standard deviation for the scale and shift map. It represents the enhancement of ability to generate accurate global structure without the help of local recovery.

Ablation Study for the Locally Weighted Linear Regression Method. The performance of our proposed local recovery strategy may be affected by the amount of sparse points, the sparsity distribution, noises from sparse points, and the bandwidth b. Their effects for the depth accuracy is explored and shown in Table 5. All experiments are conducted on the NYU dataset.

From the ablation study, we can see that simple 5×5 ground truth depth can be leveraged to recover metric depth and improve the accuracy. The more ground truth points we use, the better performance we can achieve. It is also worth mentioning that our method is robust to a uniform sample strategy and noises of ground truth, but the overly concentrated sampling strategy should be avoided in practice.

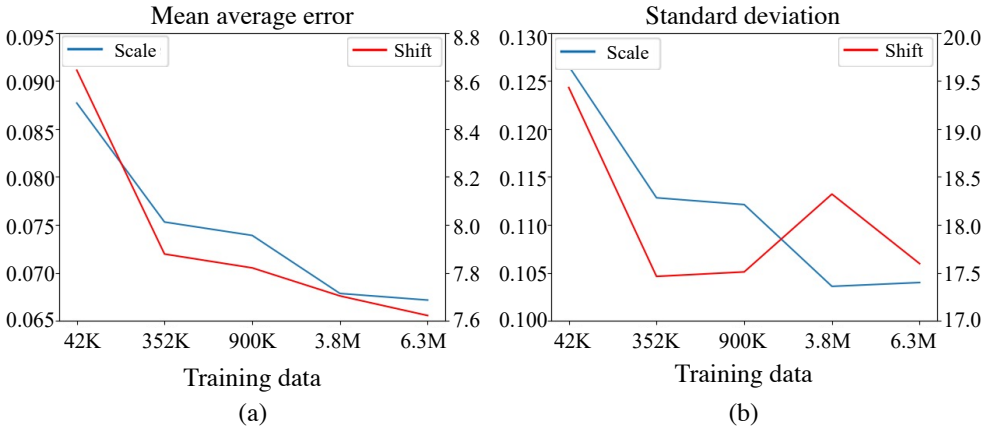

Figure 3. Analysis for the distribution of scale map and shift map. The ideal values of scale and shift are 1 and 0 separately, with which model can align metric depth well without local recovery. The overall decrease of mean average error and standard deviation shows the progressive enhancement of depth prediction.

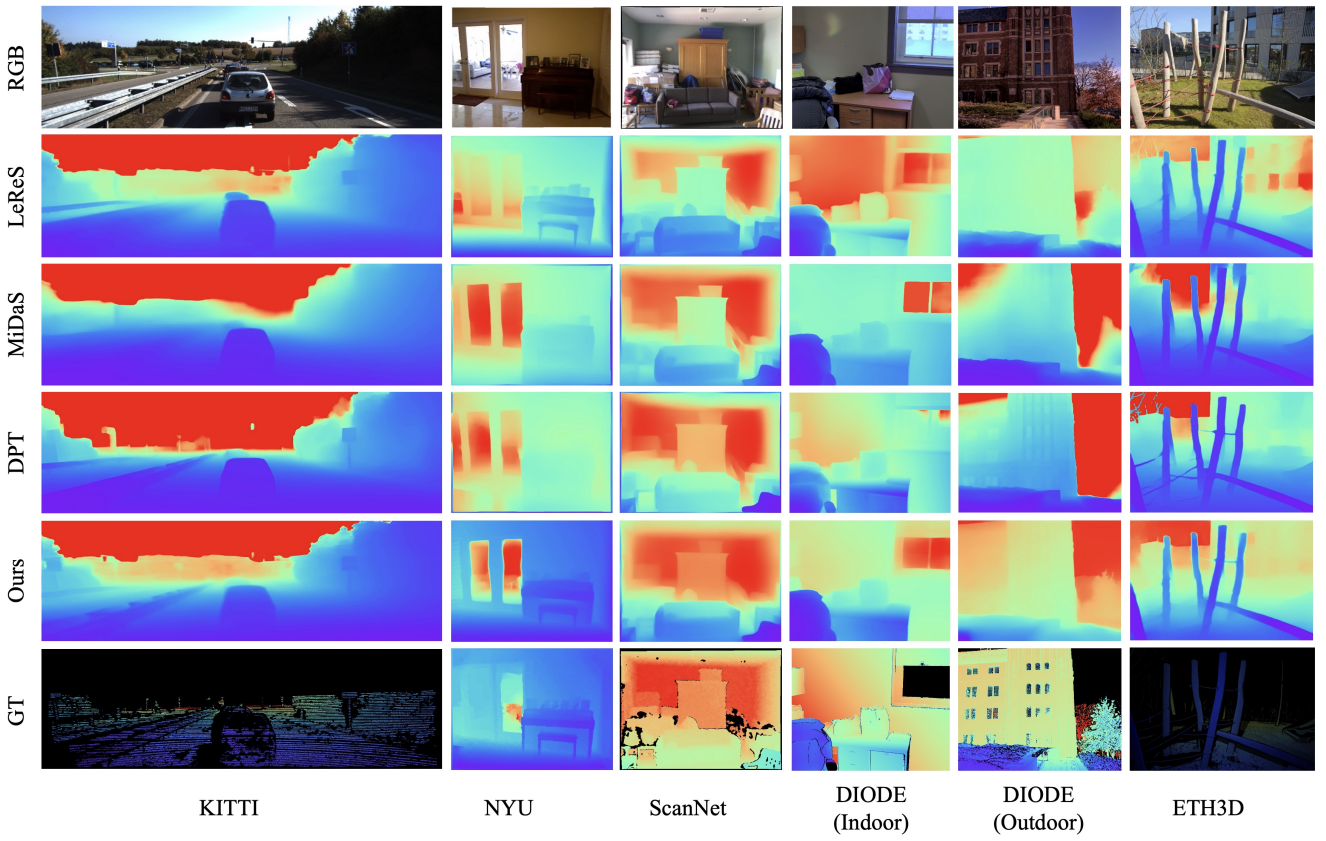

Figure 4. Qualitative comparison of depth estimation with state-of-the-art methods including LeReS [54], MiDaS [30], and DPT [29].

As for the parameter, Gaussian kernel bandwidth b, it represents the effect of distance to the weight matrix. Experimentally, we suggest to simply set parameter bandwidth to the value l/n, where l is the width of the RGB image and n is the number of sampled ground-truth points of one side. More precisely, if we sample 10×10 ground-truth points for an 500×500 image, the parameter bandwidth can be set to 50. For images with extreme aspect ratio like KITTI, l can be a compromise between them.

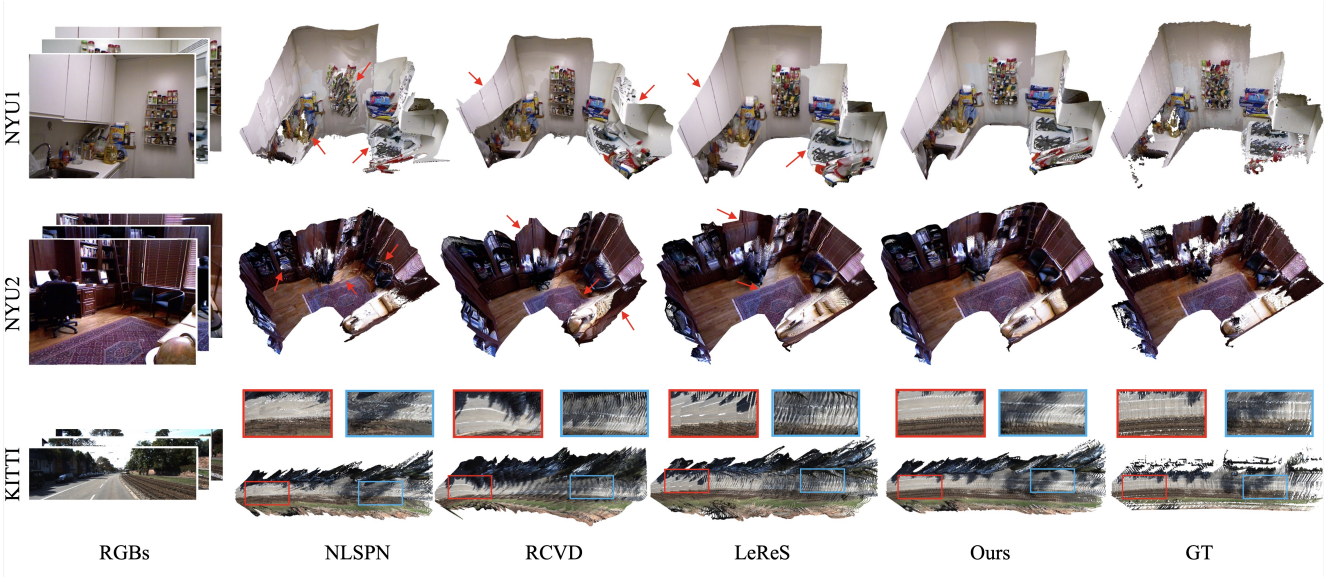

Figure 5. Qualitative comparison of 3D scene reconstruction from video. We compare with three representative methods: single image depth estimation method LeReS [54] aligned with ground truth depth, robust depth estimation method RCVD [19] with iterations of consistency optimization between frames, and depth completion method NLSPN [28] with sparse ground truth. 15% outliers of NLSPN are filtered out during visualization due to the noise of depth prediction. As the figure shows, our method reconstructs better 3D shape in both accuracy and consistency (see arrows).

Method	Basement_0001a			Bedroom_0015			Dining_room_0004			Kitchen_0008			Classroom_0004		
	AbsRel↓	δ_1↑	ADD↓	AbsRel↓	δ_1↑	ADD↓	AbsRel↓	δ_1↑	ADD↓	AbsRel↓	δ_1↑	ADD↓	AbsRel↓	δ_1↑	ADD↓
LeReS [54]	7.1	95.3	18.60	5.8	97.8	11.50	6.5	95.4	21.60	5.5	99.0	9.36	6.9	96.0	20.55
RCVD [19]	13.7	87.6	35.20	7.6	95.3	15.51	16.7	77.4	41.88	9.0	95.4	13.44	11.3	88.1	34.36
NLSPN [28]	6.6	93.7	17.47	3.3	97.3	7.85	5.7	92.6	19.24	2.7	98.6	6.00	6.0	93.1	17.35
RCVD$_{local}$	7.2	95.1	20.84	3.4	99.2	9.37	7.1	94.9	22.39	3.0	99.7	6.35	6.4	97.2	21.49
Ours$_{global}$	8.9	92.5	23.20	5.9	97.6	10.76	6.2	96.0	21.00	2.7	**99.8**	6.12	6.4	96.0	18.19
Ours$_{local}$	**5.2**	**97.1**	**15.36**	**3.1**	**98.8**	**7.51**	**3.7**	**98.1**	**16.81**	**1.6**	**99.8**	**5.33**	**4.3**	**97.5**	**14.21**

Table 6. Quantitative comparison of monocular video depth estimation with single image depth estimation, consistent video depth estimation and depth completion methods. 'ADD' is our video consistency evaluation metric proposed in Sec. 3.2. Our pipeline of 3D scene reconstruction from video achieves state-of-the-art performance on 5 NYU videos.

4.2. Video Depth Estimation and 3D Reconstruction

Video Consistency. With our well-trained model and the locally scale and shift recovery method, we can achieve high-quality video metric depth through per-frame prediction. To evaluate the consistency and accuracy of video depths, we collect 5 NYU videos and compare with the single image 3D reconstruction method (LeReS [54]), a state-of-the-art depth completion method (NLSPN [28]), and the latest robust consistent video depth estimation method (RCVD [19]). Note that only NLSPN is trained on NYU and can predict metric depth. Our method and NLSPN use the same sparse guided points (100 points). For LeReS and RCVD, we align their predictions with the ground truth metric depth globally before evaluation. The AbsRel error, δ_1, and our proposed average distortion distance error ('ADD', see Sec. 3.2) are employed for evaluation.

Comparisons are shown in Table 6. First, we compare with the depth completion method, NLSPN [28], which also uses the sparse guided points to obtain metric information. The main difference is that their model should be trained on the test set and lacks generalization in the wild. By contrast, we can achieve better performance and generalize well to zero-shot datasets due to the robust depth prior. RCVD [19] aims to solve the consistency problem for video depth prediction, and LeReS [54] performs well in the wild. Compared with them, our method achieves state-of-the-art in accuracy and consistency.

Furthermore, we conduct the qualitative comparison on NYU and KITTI. Results are shown in Fig. 5. We do the per-frame depth prediction and un-project them to the same 3D coordinate space. Depth completion method NLSPN cannot recover high-quality details. The consistency

of RCVD is much better on NYU, but the 3D structure is not accurate, see the walls. LeReS achieves excellent detail prediction but lack consistency between frames for misalignment caused by global recovery strategy. With our local recovery strategy, our method can reconstruct a better 3D point cloud than others.

5. Limitations and Discussion

We observe some limitations of our method. First, the improvement brought by local recovery strategy still relies on sparse ground truth depth, which limit the application. Second, we propose to decouple the inaccuracy and alleviate the coarse misalignment with our strategy, but ignore the detail missing inaccuracy. For future work, sparse ground truth can be replaced by some traditional geometric algorithm. High-frequency inaccuracy can be reduced by post-processing algorithms of enhancing detail information.

6. Conclusion

In this paper, we have developed a modified locally weighted linear regression strategy to significantly improve the accuracy and consistency of depth estimation, with robustness to both the amount and randomly-generated noises of the ground truth. Extensive experiments show that the proposed strategy owns significant generalization ability to monocular depth estimation and also potential practical values.

References

[1] Zuria Bauer, Francisco Gomez-Donoso, Edmanuel Cruz, Sergio Orts-Escolano, and Miguel Cazorla. Uasol, a large-scale high-resolution outdoor stereo dataset. *Scientific Data*, 6(1):1–14, 2019. 4

[2] Weifeng Chen, Zhao Fu, Dawei Yang, and Jia Deng. Single-image depth perception in the wild. In *Adv. Neural Inform. Process. Syst.*, pages 730–738, 2016. 2

[3] Weifeng Chen, Shengyi Qian, and Jia Deng. Learning single-image depth from videos using quality assessment networks. In *IEEE Conf. Comput. Vis. Pattern Recogn.*, pages 5604–5613, 2019. 2, 5

[4] Weifeng Chen, Shengyi Qian, David Fan, Noriyuki Kojima, Max Hamilton, and Jia Deng. OASIS: A large-scale dataset for single image 3d in the wild. In *IEEE Conf. Comput. Vis. Pattern Recogn.*, 2020. 2, 5

[5] Xinjing Cheng, Peng Wang, Chenye Guan, and Ruigang Yang. Cspn++: Learning context and resource aware convolutional spatial propagation networks for depth completion. In *AAAI Conf. Artificial Intelligence*, volume 34, pages 10615–10622, 2020. 2, 4

[6] Xinjing Cheng, Peng Wang, and Ruigang Yang. Learning depth with convolutional spatial propagation network. *IEEE Trans. Pattern Anal. Mach. Intell.*, 2019. 2

[7] Jaehoon Cho, Dongbo Min, Youngjung Kim, and Kwanghoon Sohn. A large rgb-d dataset for semi-supervised monocular depth estimation. *arXiv: Comp. Res. Repository*, 2019. 2

[8] Jaehoon Cho, Dongbo Min, Youngjung Kim, and Kwanghoon Sohn. Deep monocular depth estimation leveraging a large-scale outdoor stereo dataset. *Expert Systems with Applications*, 178, 2021. 4

[9] Angela Dai, Angel X Chang, Manolis Savva, Maciej Halber, Thomas Funkhouser, and Matthias Nießner. Scannet: Richly-annotated 3d reconstructions of indoor scenes. In *IEEE Conf. Comput. Vis. Pattern Recogn.*, pages 5828–5839, 2017. 2, 5

[10] Alexey Dosovitskiy, Lucas Beyer, Alexander Kolesnikov, Dirk Weissenborn, Xiaohua Zhai, Thomas Unterthiner, Mostafa Dehghani, Matthias Minderer, Georg Heigold, Sylvain Gelly, Jakob Uszkoreit, and Neil Houlsby. An image is worth 16x16 words: Transformers for image recognition at scale. *Int. Conf. Learn. Represent.*, 2021. 2, 5, 6

[11] Arda Duzceker, Silvano Galliani, Christoph Vogel, Pablo Speciale, Mihai Dusmanu, and Marc Pollefeys. DeepVideoMVS: Multi-view stereo on video with recurrent spatio-temporal fusion. In *IEEE Conf. Comput. Vis. Pattern Recogn.*, pages 15324–15333, 2021. 2

[12] Hao-Shu Fang, Chenxi Wang, Minghao Gou, and Cewu Lu. Graspnet-1billion: A large-scale benchmark for general object grasping. In *IEEE Conf. Comput. Vis. Pattern Recogn.*, pages 11444–11453, 2020. 4

[13] Andreas Geiger, Philip Lenz, and Raquel Urtasun. Are we ready for autonomous driving? the kitti vision benchmark suite. In *IEEE Conf. Comput. Vis. Pattern Recogn.*, pages 3354–3361. IEEE, 2012. 5

[14] Clément Godard, Oisin Mac Aodha, Michael Firman, and Gabriel J Brostow. Digging into self-supervised monocular depth estimation. In *Int. Conf. Comput. Vis.*, pages 3828–3838, 2019. 5, 6

[15] Kaiming He, Xiangyu Zhang, Shaoqing Ren, and Jian Sun. Deep residual learning for image recognition. In *IEEE Conf. Comput. Vis. Pattern Recogn.*, pages 770–778, 2016. 5

[16] Daniel Herrera, Juho Kannala, Janne Heikkilä, et al. Depth map inpainting under a second-order smoothness prior. In *Scandinavian Conf. Image Analysis*, pages 555–566, 2013. 2

[17] Yiwen Hua, Puneet Kohli, Pritish Uplavikar, Anand Ravi, Saravana Gunaseelan, Jason Orozco, and Edward Li. Holopix50k: A large-scale in-the-wild stereo image dataset. In *IEEE Conf. Comput. Vis. Pattern Recogn. Worksh.*, 2020. 4, 12

[18] Jingwei Huang, Zhili Chen, Duygu Ceylan, and Hailin Jin. 6-dof vr videos with a single 360-camera. In *IEEE Vir. Real.*, pages 37–44, 2017. 1

[19] Johannes Kopf, Xuejian Rong, and Jia-Bin Huang. Robust consistent video depth estimation. In *IEEE Conf. Comput. Vis. Pattern Recogn.*, 2021. 2, 8

[20] Jin Han Lee, Myung-Kyu Han, Dong Wook Ko, and Il Hong Suh. From big to small: Multi-scale local planar guidance for monocular depth estimation. *arXiv: Comp. Res. Repository*, page 1907.10326, 2019. 2

[21] Sihaeng Lee, Janghyeon Lee, Byungju Kim, Eojindl Yi, and Junmo Kim. Patch-wise attention network for monocular

depth estimation. In *AAAI Conf. Artificial Intelligence*, volume 35, pages 1873–1881, 2021. 2

[22] Zhengqi Li and Noah Snavely. Megadepth: Learning single-view depth prediction from internet photos. In *IEEE Conf. Comput. Vis. Pattern Recogn.*, pages 2041–2050, 2018. 2, 4

[23] Zhengqi Li and Noah Snavely. Megadepth: Learning single-view depth prediction from internet photos. In *IEEE Conf. Comput. Vis. Pattern Recogn.*, 2018. 5

[24] Chao Liu, Jinwei Gu, Kihwan Kim, Srinivasa G. Narasimhan, and Jan Kautz. Neural RGB $\rightarrow$ D sensing: Depth and uncertainty from a video camera. In *IEEE Conf. Comput. Vis. Pattern Recogn.*, pages 10986–10995, 2019. 2

[25] Xuan Luo, Jia-Bin Huang, Richard Szeliski, Kevin Matzen, and Johannes Kopf. Consistent video depth estimation. *ACM Trans. Graph.*, 39(4):71–1, 2020. 2

[26] Xuan Luo, Yanmeng Kong, Jason Lawrence, Ricardo Martin-Brualla, and Steven M. Seitz. Keystonedepth: History in 3d. In *Int. Conf. 3D Vis.*, November 2020. 4

[27] Kiyoshi Matsuo and Yoshimitsu Aoki. Depth image enhancement using local tangent plane approximations. In *IEEE Conf. Comput. Vis. Pattern Recogn.*, pages 3574–3583, 2015. 2

[28] Jinsun Park, Kyungdon Joo, Zhe Hu, Chi-Kuei Liu, and In So Kweon. Non-local spatial propagation network for depth completion. In *Eur. Conf. Comput. Vis.*, 2020. 2, 4, 5, 6, 8

[29] René Ranftl, Alexey Bochkovskiy, and Vladlen Koltun. Vision transformers for dense prediction. In *IEEE Conf. Comput. Vis. Pattern Recogn.*, pages 12179–12188, 2021. 1, 2, 3, 5, 6, 7

[30] René Ranftl, Katrin Lasinger, David Hafner, Konrad Schindler, and Vladlen Koltun. Towards robust monocular depth estimation: Mixing datasets for zero-shot cross-dataset transfer. *IEEE Trans. Pattern Anal. Mach. Intell.*, 2020. 1, 2, 3, 5, 6, 7

[31] Mike Roberts, Jason Ramapuram, Anurag Ranjan, Atulit Kumar, Miguel Angel Bautista, Nathan Paczan, Russ Webb, and Joshua M. Susskind. Hypersim: A photorealistic synthetic dataset for holistic indoor scene understanding. In *Int. Conf. Comput. Vis.*, 2021. 4

[32] Ashutosh Saxena, Min Sun, and Andrew Y Ng. Make3d: Learning 3d scene structure from a single still image. *IEEE Trans. Pattern Anal. Mach. Intell.*, 31(5):824–840, 2008. 2

[33] Thomas Schops, Johannes L Schonberger, Silvano Galliani, Torsten Sattler, Konrad Schindler, Marc Pollefeys, and Andreas Geiger. A multi-view stereo benchmark with high-resolution images and multi-camera videos. In *IEEE Conf. Comput. Vis. Pattern Recogn.*, pages 3260–3269, 2017. 5

[34] Nathan Silberman, Derek Hoiem, Pushmeet Kohli, and Rob Fergus. Indoor segmentation and support inference from rgbd images. In *Eur. Conf. Comput. Vis.*, pages 746–760. Springer, 2012. 2, 5

[35] Nathan Silberman, Derek Hoiem, Pushmeet Kohli, and Rob Fergus. Indoor segmentation and support inference from rgbd images. In *Eur. Conf. Comput. Vis.*, pages 746–760, 2012. 2

[36] Zachary Teed and Jia Deng. Deepv2d: Video to depth with differentiable structure from motion. In *Int. Conf. Learn. Represent.*, 2019. 2

[37] Zachary Teed and Jia Deng. Raft: Recurrent all-pairs field transforms for optical flow. In *Eur. Conf. Comput. Vis.*, pages 402–419, 2020. 12

[38] Igor Vasiljevic, Nick Kolkin, Shanyi Zhang, Ruotian Luo, Haochen Wang, Falcon Z. Dai, Andrea F. Daniele, Mohammadreza Mostajabi, Steven Basart, Matthew R. Walter, and Gregory Shakhnarovich. DIODE: A Dense Indoor and Outdoor DEpth Dataset. *arXiv:1908.00463*, 2019. 2, 5

[39] Chaoyang Wang, Simon Lucey, Federico Perazzi, and Oliver Wang. Web stereo video supervision for depth prediction from dynamic scenes. In *Int. Conf. 3D Vis.*, pages 348–357, 2019. 2, 4, 5, 12

[40] Peng Wang, Xinyu Huang, Xinjing Cheng, Dingfu Zhou, Qichuan Geng, and Ruigang Yang. The apolloscape open dataset for autonomous driving and its application. *IEEE Trans. Pattern Anal. Mach. Intell.*, 2019. 4

[41] Wenshan Wang, Delong Zhu, Xiangwei Wang, Yaoyu Hu, Yuheng Qiu, Chen Wang, Yafei Hu, Ashish Kapoor, and Sebastian Scherer. TartanAir: A dataset to push the limits of visual slam. In *Int. Conf. Intell. Rob. & Syst.*, 2020. 4

[42] Yan Wang, Wei-Lun Chao, Divyansh Garg, Bharath Hariharan, Mark Campbell, and Kilian Weinberger. Pseudo-lidar from visual depth estimation: Bridging the gap in 3d object detection for autonomous driving. In *IEEE Conf. Comput. Vis. Pattern Recogn.*, 2019. 1

[43] Ke Xian, Chunhua Shen, Zhiguo Cao, Hao Lu, Yang Xiao, Ruibo Li, and Zhenbo Luo. Monocular relative depth perception with web stereo data supervision. In *IEEE Conf. Comput. Vis. Pattern Recogn.*, pages 311–320, 2018. 2, 12

[44] Ke Xian, Jianming Zhang, Oliver Wang, Long Mai, Zhe Lin, and Zhiguo Cao. Structure-guided ranking loss for single image depth prediction. In *IEEE Conf. Comput. Vis. Pattern Recogn.*, pages 611–620, 2020. 2, 5

[45] Ke Xian, Jianming Zhang, Oliver Wang, Long Mai, Zhe Lin, and Zhiguo Cao. Structure-guided ranking loss for single image depth prediction. In *IEEE Conf. Comput. Vis. Pattern Recogn.*, June 2020. 4

[46] Enze Xie, Wenhai Wang, Zhiding Yu, Anima Anandkumar, Jose M Alvarez, and Ping Luo. SegFormer: Simple and efficient design for semantic segmentation with transformers. In *Adv. Neural Inform. Process. Syst.*, 2021. 12

[47] Saining Xie, Ross Girshick, Piotr Dollár, Zhuowen Tu, and Kaiming He. Aggregated residual transformations for deep neural networks. In *IEEE Conf. Comput. Vis. Pattern Recogn.*, pages 1492–1500, 2017. 5

[48] Guorun Yang, Xiao Song, Chaoqin Huang, Zhidong Deng, Jianping Shi, and Bolei Zhou. Drivingstereo: A large-scale dataset for stereo matching in autonomous driving scenarios. In *IEEE Conf. Comput. Vis. Pattern Recogn.*, 2019. 4

[49] Xingbin Yang, Liyang Zhou, Hanqing Jiang, Zhongliang Tang, Yuanbo Wang, Hujun Bao, and Guofeng Zhang. Mobile3DRecon: real-time monocular 3D reconstruction on a mobile phone. *IEEE Trans. Vis. and Comp. Graph.*, 26(12):3446–3456, 2020. 1

[50] Yanchao Yang, Alex Wong, and Stefano Soatto. Dense depth posterior (ddp) from single image and sparse range. In *IEEE Conf. Comput. Vis. Pattern Recogn.*, pages 3353–3362, 2019. 2

[51] Wei Yin, Yifan Liu, and Chunhua Shen. Virtual normal: Enforcing geometric constraints for accurate and robust depth prediction. *IEEE Trans. Pattern Anal. Mach. Intell.*, 2021. 2, 3, 5

[52] Wei Yin, Yifan Liu, Chunhua Shen, and Youliang Yan. Enforcing geometric constraints of virtual normal for depth prediction. In *Int. Conf. Comput. Vis.*, 2019. 2, 5, 6

[53] Wei Yin, Xinlong Wang, Chunhua Shen, Yifan Liu, Zhi Tian, Songcen Xu, Changming Sun, and Dou Renyin. Diversedepth: Affine-invariant depth prediction using diverse data. *arXiv: Comp. Res. Repository*, page 2002.00569, 2020. 2, 3, 4

[54] Wei Yin, Jianming Zhang, Oliver Wang, Simon Niklaus, Long Mai, Simon Chen, and Chunhua Shen. Learning to recover 3d scene shape from a single image. In *IEEE Conf. Comput. Vis. Pattern Recogn.*, 2021. 1, 2, 3, 4, 5, 6, 7, 8, 12

[55] Amir R Zamir, Alexander Sax, William Shen, Leonidas J Guibas, Jitendra Malik, and Silvio Savarese. Taskonomy: Disentangling task transfer learning. In *IEEE Conf. Comput. Vis. Pattern Recogn.*, pages 3712–3722, 2018. 2

[56] Amir R. Zamir, Alexander Sax, William B. Shen, Leonidas J. Guibas, Jitendra Malik, and Silvio Savarese. Taskonomy: Disentangling task transfer learning. In *IEEE Conf. Comput. Vis. Pattern Recogn.* IEEE, 2018. 4, 12

[57] Yinda Zhang and Thomas Funkhouser. Deep depth completion of a single rgb-d image. *IEEE Conf. Comput. Vis. Pattern Recogn.*, 2018. 2

Appendix

We provide more information here.

A. Datasets for Training

During training, we collect over 6.3 million data to improve the robustness of our monocular depth estimation model. These datasets are separated into high-quality, mid-quality and mid-stereo following [54], and are processed as follows:

For low-quality web-stereo data, such as WSVD [39] and HoloPix50k [17], we follow [39, 43] to employ an optical flow method, RAFT [37], to obtain the relative depth. Frames are sampled every 3 seconds for WSVD videos. For the high-quality Taskonomy [56], we employ the least-square fitting to recover also possible instance planes, which are used in the pair-wise normal regression loss [54]. Furthermore, we employ the latest semantic segmentation method, Segformer [46], to separate the sky regions in all data and set them with the largest depth value during training.

B. Analysis of the Amount of Ground-truth Points

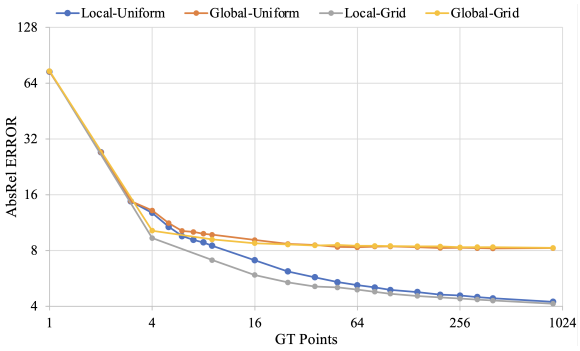

Figure S1. Comparison of local and global recovery strategy of predicted depth, uniform and grid sample strategy of GT points during recovering monocular metric depth. With our proposed local recovery, the performance of monocular depth estimation improves significantly with the increase of GT points. Also, the grid sampling strategy outperforms the uniform one, which can reduce the requirements for GT points.

We conduct detailed analysis for the amount of ground-truth points, with global recovery and local recovery separately. Sampling strategies of grid and uniform are also performed. As shown in Table S1, the AbsRel error of predicted depth aligned through local recovery decrease more obviously than that of global recovery, and the grid sample strategy can achieve better performance compared with uniform strategy. Intuitive comparison is also illustrated in Fig. S1.

GT Points	Local-Uniform	Global-Uniform	Local-Grid	Global-Grid
	AbsRel Error↓			
1	73.84	73.84	74.43	74.43
2	27.1	27.1	-	-
3	14.73	14.78	-	-
4	12.77	13.15	9.33	10.23
5	10.73	11.23	-	-
6	9.56	10.2	-	-
7	9.13	10.07	-	-
8	8.85	9.85	-	-
9	8.49	9.74	7.1	9.18
16	7.09	9.11	5.9	8.76
25	6.17	8.68	5.38	8.62
36	5.74	8.56	5.12	8.52
49	5.4	8.36	5.06	8.58
64	5.2	8.33	4.92	8.49
81	5.06	8.4	4.79	8.48
100	4.9	8.41	4.68	8.46
144	4.78	8.34	4.55	8.43
196	4.62	8.26	4.47	8.42
256	4.57	8.28	4.4	8.33
324	4.49	8.24	4.35	8.35
400	4.42	8.21	4.3	8.34
900	4.23	8.24	4.13	8.27

Table S1. Analysis for the amount of ground-truth (GT) points during recovering monocular metric depth. 'Global' and 'Local' represent global recovery and local recovery strategy separately. 'Grid' and 'Uniform' stand for sampling from grid and uniformly. The AbsRel error decrease faster with our proposed local recovery strategy with the increase of GT points.

C. Analysis for Depth Error Map and Efficiency of Local Recovery Strategy

In Fig. S3, we visualize the error map between ground truth depth and predicted depth aligned through global recovery (see 'Global Error' row) and local recovery (see 'Local Error' row) separately. The local recovery strategy can generate an oppositely distributed scale map (see 'Scale Map' row) and a fine-tune shift map (see 'Shift Map' row) to alleviate the coarse misalignment of predicted depth. Our proposed local recovery strategy also improves the linear relation of prediction-GT pairs (compare 'Local Curve' row with 'Global Curve' row).

D. Illustration of the 3D Point Cloud

We illustrate some examples of 3D point cloud unprojected from our proposed per-frame monocular video depth estimation pipeline in Fig. S2. The video depth is predicted by monocular depth estimation module and aligns consistent metric depth between frames by sparse GT points.

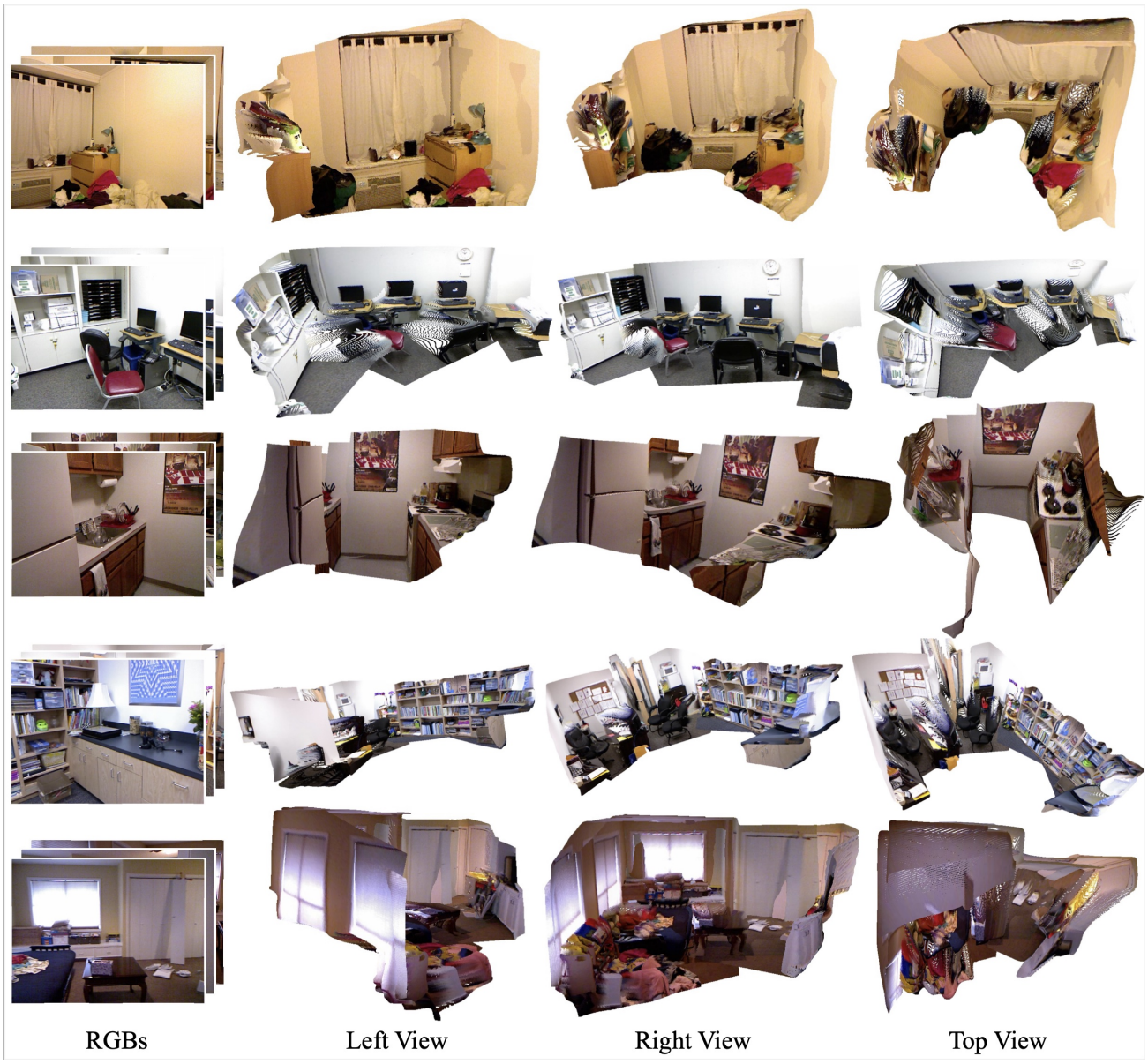

Figure S2. Illustration of the reconstructed 3D point cloud. The columns show the input RGB videos and point cloud un-projected from left, right, top view separately.

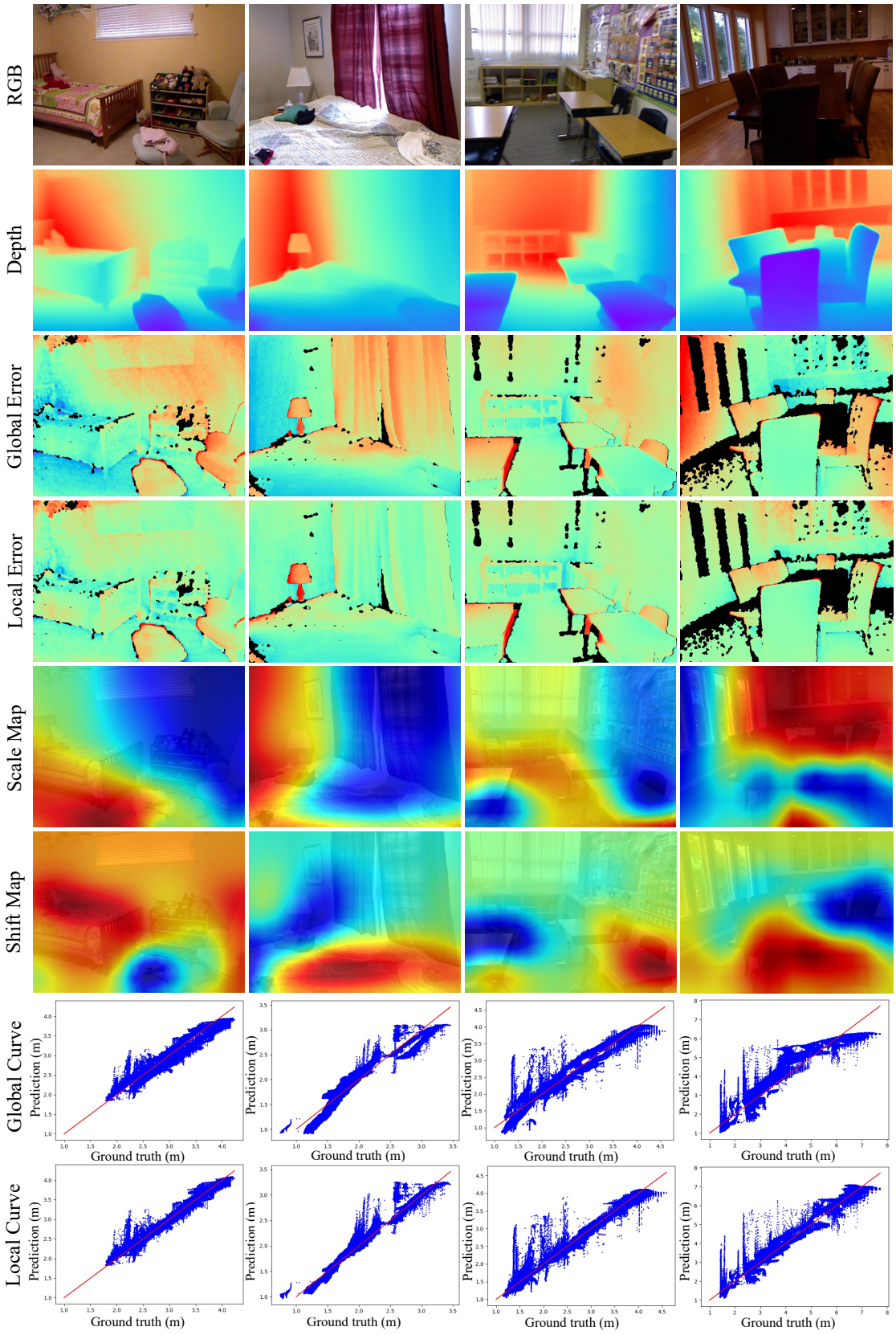
RGB
Depth
Global Error
Local Error
Scale Map
Shift Map
Global Curve
Local Curve
Prediction (m)
Ground truth (m)

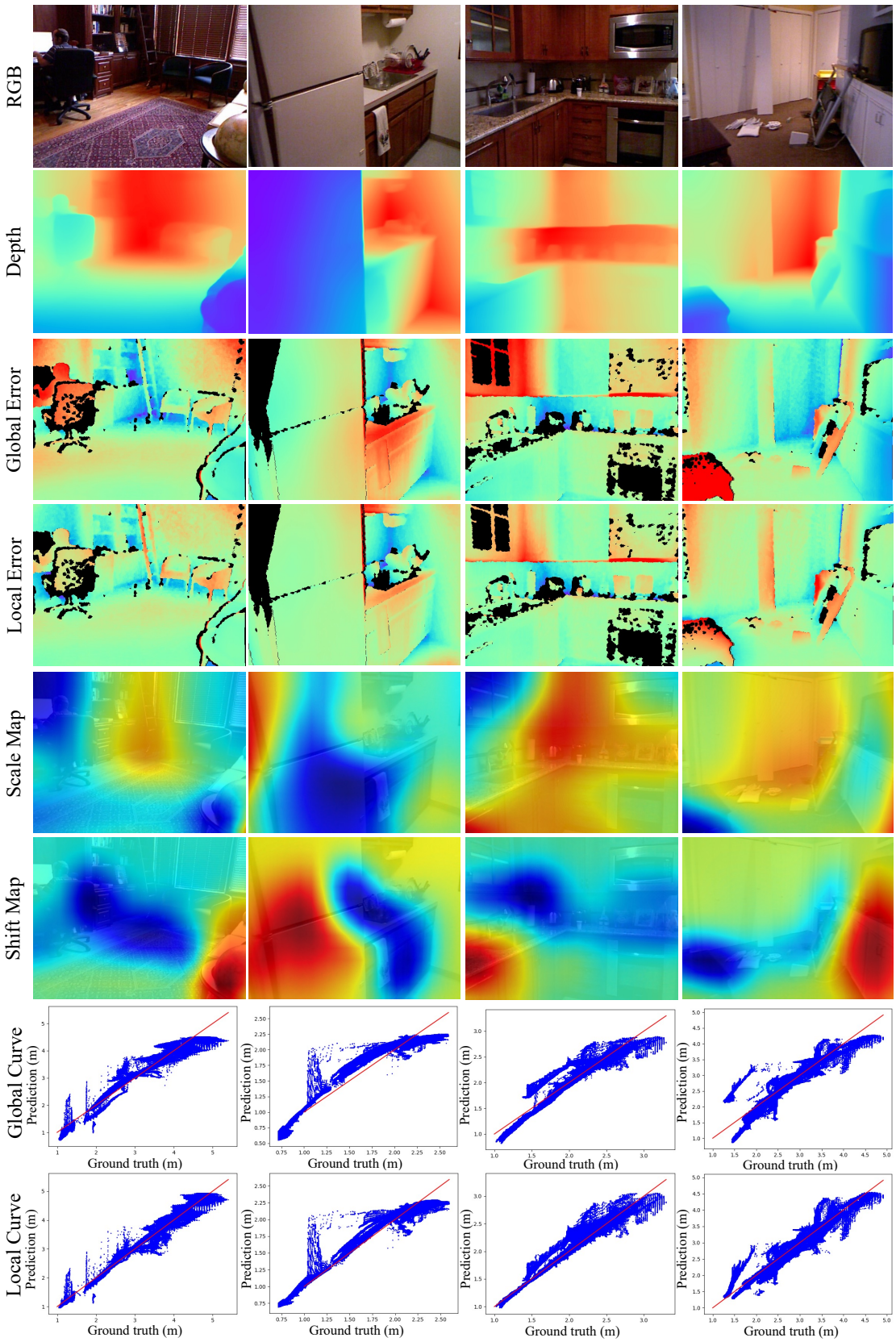

Figure S3. Analysis for depth error map, scale map and prediction-GT curve of monocular depth estimation. Our proposed local recovery strategy can generate an oppositely distributed scale map compared with error map of global recovery, which can alleviate the coarse misalignment of predicted depth and improve the linear relation of prediction-GT pairs.